

## Selective area growth rates of III-V nanowires

Martin Espiñeira Cachaza <sup>1,2,\*</sup>, Anna Wulff Christensen,<sup>1,2,\*</sup> Daria Beznasyuk,<sup>1,2</sup> Tobias Særkjær,<sup>1,2</sup> Morten Hannibal Madsen,<sup>2</sup> Rawa Tanta,<sup>2</sup> Gunjan Nagda,<sup>1,2</sup> Sergej Schuwalow,<sup>1,2</sup> and Peter Krogstrup<sup>1,2,†</sup>

<sup>1</sup>Microsoft Quantum Materials Lab Copenhagen, 2800 Lyngby, Denmark

<sup>2</sup>Center for Quantum Devices, Niels Bohr Institute, University of Copenhagen, 2100 Copenhagen, Denmark



(Received 25 July 2021; accepted 20 August 2021; published 1 September 2021)

Selective area growth (SAG) of semiconductors is a scalable method for fabricating gate-controlled quantum platforms. This letter reports on the adatom diffusion, incorporation, and desorption mechanisms that govern the growth rates of SAG nanowire (NW) arrays. We propose a model for the crystal growth rates that considers two parameter groups: the crystal growth control parameters and the design parameters. Using GaAs and InGaAs SAG NWs as a platform, we show how the design parameters such as NW pitch, width, and orientation have an impact on the growth rates. We demonstrate that by varying the control parameters (i.e., substrate temperature and beam fluxes) source, balance, and sink growth modes may exist in the SAG selectivity window. Using this model, we show that inhomogeneous growth rates can be compensated by tuning the design parameters.

DOI: [10.1103/PhysRevMaterials.5.094601](https://doi.org/10.1103/PhysRevMaterials.5.094601)

### I. INTRODUCTION

One-dimensional semiconductor nanowires (NWs) have the potential to become the host platform of future quantum information technologies [1–4]. Among the different crystal growth techniques of semiconductor NWs [5–9], selective area growth (SAG) of in-plane III-V NWs using molecular beam epitaxy (MBE) is a method for synthesizing scalable gate-controlled one-dimensional quantum electronics [10,11]. In particular, the design flexibility allows for arbitrary device architectures including networks of quantum dots and NWs.

Recently, in-plane III-V NW arrays have gained attention and have been demonstrated with a variety of materials, shapes, and dimensions [12–21]. Optimizing SAG crystal growth for the functionality and quality of such quantum structures implies optimizations of the morphology [17], composition [22], crystal disorder [23–25], and strain uniformity [26]. This makes it necessary to control the incorporation rates with high precision in order to optimize the performance of quantum devices [27,28].

Here we present a study of adatom incorporation during crystal growth of in-plane GaAs and InGaAs SAG NWs, grown by MBE on GaAs(001) and InP(001) substrates. A silicon dioxide (SiO<sub>2</sub>) mask is used to define NWs on the substrates [12]. We discuss two groups of parameters that affect SAG NW growth rates: *growth control* parameters, namely substrate temperature ( $T_{\text{sub}}$ ) and beam fluxes ( $f_i$ ), and the *NW design* such as the width ( $w$ ), interwire pitch ( $p$ ), and in plane crystallographic orientation [ $hkl$ ]. These dependencies are of importance for the design of reproducible arrays of NWs.

### II. ADATOM KINETICS

A crystal growth by MBE is facilitated by incoming beam fluxes of growth species that impinge and get adsorbed on the substrate surface [29–31]. We describe this mechanism by transition-state kinetics of the adatoms, where the transition rates  $\Gamma_{\alpha\beta}$  ( $\alpha$  and  $\beta$  denote the initial and final state, respectively) are limited by effective kinetic barriers [32]. To achieve SAG, the adatoms on the mask must either desorb or diffuse to the exposed crystal areas. The crystal growth rate is highly dependent on  $T_{\text{sub}}$  and  $f_i$ , as well as the surface-state parameters, e.g., activation energies for adatom desorption, surface diffusion, nucleation, and incorporation [21]. Following the continuum kinetics approach in Ref. [32] and ignoring adatom chemical potential variations, the transition rates can be described by the Arrhenius equation  $\Gamma_{\alpha\beta} \propto \rho_{\alpha} \exp(-\frac{\delta g_{\alpha\beta}}{k_B T_{\text{sub}}})$ , where  $k_B$  is the Boltzmann constant,  $\rho_{\alpha}$  is the adatom density in the initial state, and  $\delta g_{\alpha\beta}$  is the effective activation energy for the transition.

Figure 1(a) sketches the different types of adatom transitions which take place during SAG: adatom diffusion on either the mask surface ( $\Gamma_{a_m a_m}$ ), the growing crystal surface ( $\Gamma_{a_c a_c}$ ) or across a mask-crystal boundary ( $\Gamma_{a_m a_c}$ ); adatom incorporation into the crystal solid phase ( $\Gamma_{a_c s}$ ), or via nucleation to solid phase on the mask ( $\Gamma_{a_m s}$ ); or adatom desorption from the mask ( $\Gamma_{a_m v}$ ) and crystal ( $\Gamma_{a_c v}$ ) to vapor. All transition rates in this study are effective rates describing the mean properties of the transitions, e.g.,  $\Gamma_{a_c s}$  describes both the nucleation limited transitions as well as potential single atomic barriers for incorporation. Due to the geometry, the mask-crystal boundary is one dimensional (1D) like (linear) and the boundary of the  $\Gamma_{a_c s}$ ,  $\Gamma_{a_c v}$ ,  $\Gamma_{a_m s}$ , and  $\Gamma_{a_m v}$  transitions is 2D like (surface).

The total current of adatoms of species  $i$  being incorporated in a NW segment of length  $l$  and width  $w$  ( $l \gg w$ ) is given by adatom conservation:

$$I_{a_c s, i} = (f_i - \Gamma_{a_c v, i})wl + (\Gamma_{a_m a_c, i} - \Gamma_{a_c a_m, i})2l, \quad (1)$$

\*These authors contributed equally to this work.

†Corresponding author: krogstrup@nbi.dk

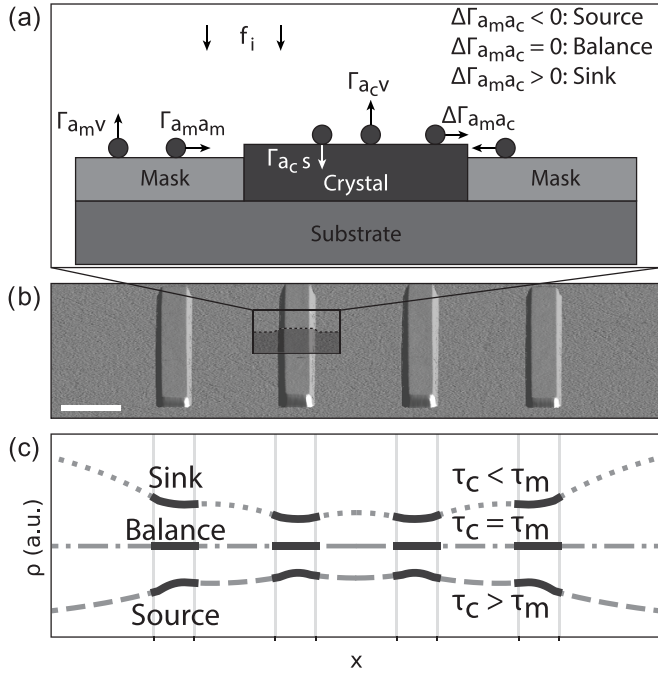


FIG. 1. (a) Schematic of adatom transitions during SAG. (b) AFM image of four parallel GaAs NWs oriented along the  $[1\bar{1}0]$  crystal orientation on a GaAs (001) substrate. Scale bar is 500 nm. (c) Three types of solutions to the simulation of coupled diffusion equations describing the adatom density on four parallel NWs assuming infinite length. The dashed and solid lines are the adatom density on mask and crystal regions, respectively.

assuming no substrate decomposition  $\Gamma_{sac} = 0$ . From mass conservation, the incorporation rate on the SAG NW can therefore be written as

$$\Gamma_{acs} = \sum_i f_i - \Gamma_{acv,i} + 2 \frac{\Gamma_{ama_c,i} - \Gamma_{acm,i}}{w}. \quad (2)$$

Then the crystal volume growth rate is  $\Gamma_{acs} \cdot \Omega$ , where  $\Omega$  is the volume of a III-V atomic pair. While  $f_i$  is a controlled parameter, the desorption term  $\Gamma_{acv,i}$  is highly dependent on  $T_{\text{sub}}$ . Thus, if the desorption from the crystal can be ignored for a given  $T_{\text{sub}}$ , i.e.,  $\Gamma_{acv} = 0$ , then the relevant term for controlling the growth rate is the flux across the mask-crystal boundary,

$$\Delta \Gamma_{ama_c,i} = \Gamma_{ama_c,i} - \Gamma_{acm,i}, \quad (3)$$

where the forward flux  $\Gamma_{ama_c,i}$  is the flux of adatoms to the crystal collected from the mask and the backward flux  $\Gamma_{acm,i}$  is the flux of adatoms to the mask collected from the crystal. We define the growth mode as *source* if  $\Delta \Gamma_{ama_c,i} < 0$ , *sink* if  $\Delta \Gamma_{ama_c,i} > 0$ , and *balance* if  $\Delta \Gamma_{ama_c,i} = 0$ .

To simulate the adatom fluxes in this system, we start by simplifying the adatom diffusion problem to one dimension by considering only the transversal direction  $x$  of an array of parallel NWs of infinite  $l$ . The steady-state adatom diffusion

equation for each surface  $j$  can be written as

$$D_j \frac{\partial^2 \rho_j(x)}{\partial x^2} + f - \Gamma_{ajv}(x) - \Gamma_{ajs}(x) = 0, \quad (4)$$

where the mask and crystal surfaces  $j$  are coupled via boundary conditions for the particular design in question. We consider four NWs in parallel with symmetry at the midpoint between the two inner NWs ( $x = 0$ ) and at  $x = \infty$ , i.e.,  $\frac{\partial \rho_j}{\partial x} = 0$  (see Supplemental Material S1 [33]). Figure 1(b) is an atomic force microscopy (AFM) image of a typical array of four NWs used in this work. At the boundaries, we assume continuity,  $\rho_c = \rho_m$ , and mass conservation,  $D_c \frac{\partial \rho_c}{\partial x} = D_m \frac{\partial \rho_m}{\partial x}$ . Since the effective incorporation rate is proportional to the adatom density,  $\Gamma_{acs} \propto \rho_c \exp(-\frac{\delta g_{acs}}{k_B T})$ , we are interested in solving  $\rho_c$  as a measure of the SAG growth rate. The model exhibits three general types of solutions, shown in Fig. 1(c): Sink, balance, and source growth modes. If there is no adatom desorption from the crystal  $\Gamma_{acv} = 0$ , then the sink (source) mode implies that the NW growth rate is higher (lower) than the calibrated corresponding planar growth rate (2D-like growth with no mask), due to an inhomogeneous flux of adatoms  $\Gamma_{ama_c}$  at the boundary. The balance mode implies that the NW growth rate is equal to the corresponding planar growth rate, and, importantly, it is *independent of NW design*. These distinct growth modes have implications for the design of NW patterns. In the following, we will explore SAG growth rates of GaAs and InGaAs based NWs grown on GaAs and InP substrates with a  $\text{SiO}_2$  mask and illustrate how growth modes and growth rates can be identified and quantified.

### III. EXPERIMENTAL METHODS

The structures under study consist of individual NWs and arrays of NWs, with varying pitch and width. The NWs are 14- $\mu\text{m}$ -long and to avoid influence from the ends, the measure of incorporation is only considered in the central region of the NW (see Supplemental Material S2 [33]). The employed  $\text{SiO}_2$  mask fabrication flow and crystal growth concept by MBE are described in Refs. [12,34], respectively. Supplemental Material S3 [33] contains information about the typical roughness of mask and substrate prior MBE growth. The MBE beam fluxes are calibrated to the corresponding planar growth rates using reflection high energy electron diffraction (RHEED) oscillations under conditions where desorption of group III can be ignored [21]. We calibrate the V:III 1:1 flux ratio with the surface reconstruction change procedure, using RHEED on GaAs(100) substrates [35,36]. Temperature is measured with pyrometer, which is calibrated with GaAs oxide desorption [37]. After growth, the SAG NW volume in single layer growths is measured by AFM and the cross-sectional area on the multilayer sample is measured by cross-sectional transmission electron microscopy (TEM). We define the NW growth rate,  $\Gamma_{\text{inc}}$ , as the measured crystal volume divided by the volume of a NW section with the same  $w$  and  $l$  from the equivalent planar growth used for the flux calibration.  $\Gamma_{\text{inc}}$  is a measure of the amount of material incorporated in a NW compared to the 2D growth and hence the effect on material incorporation caused by the mask-crystal interface term  $\Delta \Gamma_{ama_c}$  from Eq. (2). The mask selectivity measurements

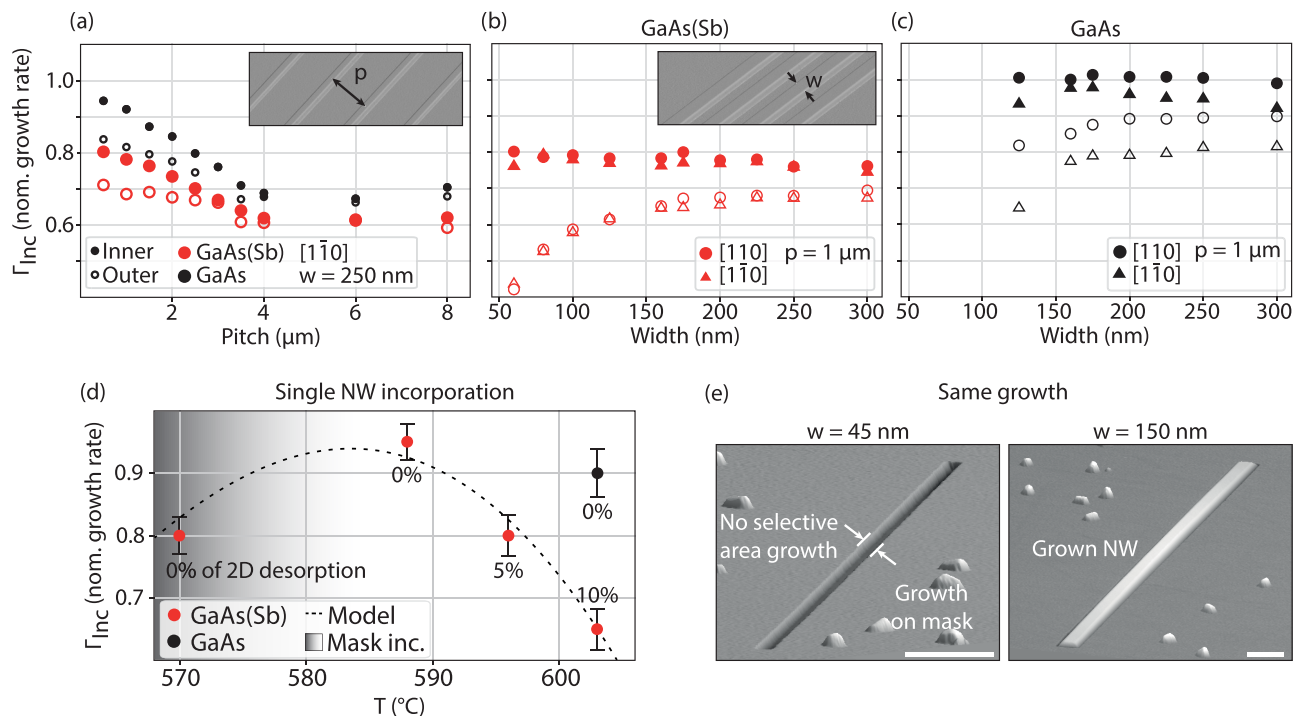


FIG. 2. NW Incorporation rate dependence on design parameters, pitch, width, and  $[hkl]$ . Incorporation rates in (a)–(c) are measured in units of nominal growth rate of GaAs and GaAs(Sb). All three plots share the same y scale. Filled (open) points indicate incorporation rates measured on the inner (outer) NWs. GaAs(Sb) is shown by red symbols, and GaAs by black symbols. (a) Incorporation rates of inner and outer NWs in a four-NWs array, as a function of NW  $p$ . The inset shows an AFM image of an example array. Panels (b) and (c) are the incorporation rates of GaAs(Sb) and GaAs, respectively, as a function of  $w$  and for  $[110]$  and  $[1\bar{1}0]$  oriented NWs. The inset in (b) is an AFM image of an example array. (d) Incorporation of isolated NWs as a function of  $T_{\text{sub}}$  indicated by black (red) symbols, for GaAs [GaAs(Sb)]. The dashed line is extracted from the model based on Eq. (2), highlighting a maximum incorporation near  $583^\circ\text{C}$ . The number below each data point corresponds to the percentage of desorbed material from the crystal  $\Gamma_{a_c,v}$ , measured on large mask openings. The blurred gray background represent the transition from  $\Gamma_{a_{ms}} = 0$  (white) to  $>0$  (gray). (e) Example of individual isolated 45- and 150-nm-wide NWs, both from the same GaAs(Sb) growth. The source effect overrides the growth inside the 45-nm trench due to its width limitation, whereas the 150 nm grows as expected. Scale bars are 200 nm.

are performed in areas with no mask openings, to avoid any influence from the  $\Delta\Gamma_{a_{ms}}$  term.

#### IV. RESULTS AND DISCUSSIONS

We start by examining the growth rates in arrays of four parallel NWs, shown in Figs. 2(a) and 2(b) insets, as a function of design parameters  $p$ ,  $w$ , and  $[hkl]$ . We determine the growth mode by comparing incorporation rates between the two inner and two outer NWs. Figures 2(a)–2(c) shows the mean incorporation rate of pure GaAs and Sb surfactant-aided GaAs(Sb) NWs grown on a GaAs(001) substrate at  $T_{\text{sub}}$  of  $603^\circ\text{C}$ . The Ga flux corresponds to a planar GaAs growth rate of 0.1 monolayers (ML)/s, under As rich conditions (see Supplemental Material S4 for recipe details [33]). The reason for the selection of these two materials is their use as buffer layers before the growth on InAs transport channels, due to its beneficial effect of crystal defect reduction at the InAs interface [12]. In Fig. 2(a) the mean incorporation rates of inner and outer NWs is plotted as a function of  $p$  for  $[1\bar{1}0]$  orientated NWs of  $w = 250$  nm. The data reveal a decrease in incorporation rates with increasing  $p$  until it saturates at around  $4\ \mu\text{m}$  for both GaAs and GaAs(Sb) to 0.7 and 0.6 of the nominal incorporation rate, respectively. We note that the  $[1\bar{1}0]$  NWs

exhibit different faceting with and without Sb surfactant, with (001) vertical and  $\{113\}$  side predominant facets, respectively [38] (more details about faceting in Supplemental Material S2 [33]). The different faceting can affect the total incorporation of the NW due to Ga adatom diffusion length  $\lambda_{\text{Ga},c}$  anisotropy on GaAs(001) [39]. However, in the  $p$  study we consider this effect negligible since  $w \ll \lambda_{\text{Ga},c[110]}$  and  $\lambda_{\text{Ga},c[1\bar{1}0]}$  [40,41]. The facet time evolution of GaAs NWs from initial (001) to  $\{113\}$  is not considered because the initial stages of the growth are dominated by the diffusion on the original (001) substrate and the NWs reach the  $\{113\}$  fully grown facets at the end of the growth process. The incorporation rate of pure GaAs arrays approaches the nominal value (i.e.,  $\Gamma_{\text{inc}} = 1$ ) at small  $p$ , as expected if the desorption from the crystal is negligible, i.e.,  $\Gamma_{a_c,v,\text{Ga}} \approx 0$ . By contrast, GaAs(Sb) NWs have a lower incorporation rates but with the same overall trend. This general downwards shift of  $\sim 10\%$  in the incorporation curve for the Sb surfactant compared with the pure case can be explained by two reasons: a result of nonreactive surfactants nature, which decrease the number of incorporation sites for adatoms [42,43] and the higher facet roughness of  $\{113\}$  compared to (001). The decrease in incorporation with pitch implies that the growth is in the source mode ( $\Delta\Gamma_{a_{ms}} < 0$ ). As a consequence, an increasing pitch implies a decreasing

number of adatoms being shared between neighboring NWs before they are desorbed from the mask. In the regime of significantly large pitch ( $p \gg \lambda_{\text{Ga},m}$ ) [10,44], the sourcing of adatoms between NWs can be ignored. All NWs in the array grow at the same rate and can be considered decoupled from each other. In this regime, the amount of material incorporated by a NW compared to the nominal growth rate is a direct measure of the source mode strength for the given growth conditions.

While the  $p$  dependence is used to study the desorption limited  $\lambda_{\text{Ga},m}$ , the  $w$  dependence can be used to study the incorporation limited  $\lambda_{\text{Ga},c}$ . Figures 2(b) and 2(c) show the incorporation rate as a function of  $w$ , with and without Sb surfactant respectively, for both [110] and [1 $\bar{1}$ 0] oriented NW arrays with  $p = 1 \mu\text{m}$ . As shown in Fig. 2(b), the GaAs(Sb) growth rate is independent of  $[hkl]$  and even independent of  $w$  for the inner NWs. However, for the outer NWs there is a decrease in the growth rate with decreasing  $w$ . The outer NW growth rate dependence on  $w$  is consistent with Eq. (2); as  $w$  increases the sourcing effect from  $\Delta\Gamma_{a_m a_c}$  becomes negligible for the given NW, and the incorporation rate converges toward  $\Gamma_{a_c s} = f_i - \Gamma_{a_c v, i}$ . If  $\Gamma_{a_c v, \text{Ga}} \approx 0$  and the width approaches  $w \gg \lambda_{\text{Ga},c}$ , then the mean incorporation rate will converge toward the nominal growth rate for all NWs in the array, ignoring the effect of the surfactant. For increasing widths the growth rate converges toward 0.7–0.8 of the nominal growth rate, which can be explained with a longer  $\tau_{\text{Ga},c}$  due to the role of the surfactant and therefore a higher  $\Gamma_{a_c a_m}$ . On the other hand, the apparent  $w$  independence on incorporation for the inner GaAs(Sb) NWs is not obvious. We speculate that this apparent independence of  $\Gamma_{\text{inc}}$  is due to a compensation on growth rates. The inner NWs get more sourced adatoms from its neighbors, as the outer NWs incorporate less at smaller  $w$ . The  $\Gamma_{\text{inc}}$  difference between both inner and outer NWs on both directions with  $w = 150\text{--}300 \text{ nm}$  slowly decreases and it is expected to merge at larger  $w$ . In Fig. 2(c), there is a clear dependence on  $[hkl]$  and the incorporation rate of GaAs is more efficient on the crystal with  $\Gamma_{\text{inc}}$  closer to 1. As the NWs grow, the faceting evolves differently depending on the NW orientation, which means that  $\lambda_{\text{Ga},c}$  also changes during growth. Thus, the crystal surface parameters can be dynamic in nature. The NWs oriented along [1 $\bar{1}$ 0] form dominating {113} facets, while the [110] oriented NWs preserve the (001) top facet. As such, the [1 $\bar{1}$ 0]-oriented NWs exhibit a stronger source effect because the longer lifetime results in a lower incorporation rate, and therefore a more negative  $\Delta\Gamma_{a_m a_c}$  compared to the NWs oriented along [110]. This is consistent with the findings in reference [45] which show the incorporation rate of Ga on {113} GaAs facets is slower than on (001). As we are measuring only mean growth rates, for simplicity we also assume constant surface-state parameters for the modeling, and any change in faceting during the growth is not considered.

The growths discussed in the previous paragraphs exhibit a source behavior. To answer if it is possible to manipulate the strength of the source effect  $\Delta\Gamma_{a_m a_c}$ , and potentially achieve balanced and sink growth modes, we grow four identical GaAs(Sb) samples where only  $T_{\text{sub}}$  is varied between 570 °C and 603 °C at a nominal growth rate of 0.1 ML/s with a V/III ratio of 9. As shown in Ref. [46], the reduction of  $T_{\text{sub}}$  leads

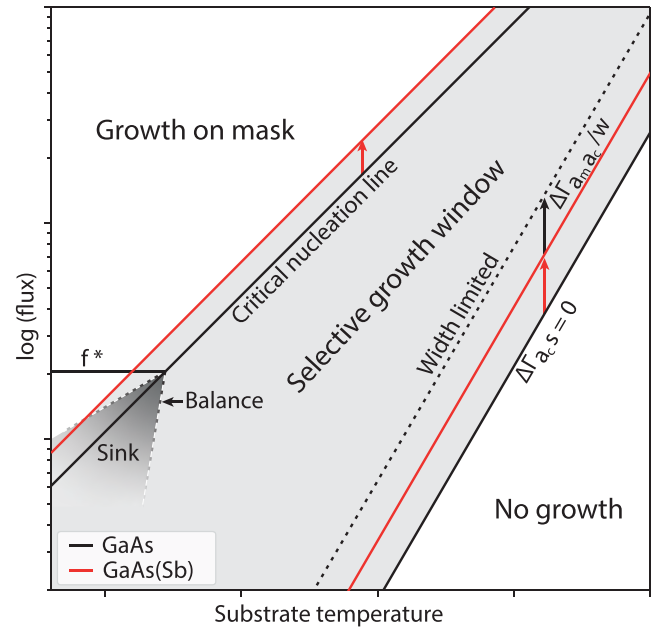


FIG. 3. Sketch of SAG growth window and the implications of the source effect. The transition from solid black to solid red lines indicated by the red arrows is caused by the use of Sb surfactant during growth, shifting the  $\Gamma_{a_c s} = 0$  and  $\Gamma_{a_m s} = 0$  lines toward lower  $T$ . The transition from solid red to dotted black on the  $\Gamma_{a_c s} = 0$  line is caused by the width limitation of the design, additionally shifting it toward lower  $T$ . A region of sink growth mode may exist at low  $f$  and  $T$ , delimited by a line that would be balanced growth mode. Above the sink region maximum flux  $f^*$ , all growths are expected to be in source mode.

to an exponential reduction of  $\Gamma_{a_m v}$ , decreasing  $\Gamma_{a_c a_m}$  since the adatom density will be higher on the mask. Incorporation rates are measured on isolated NWs of  $w = 250 \text{ nm}$  for each growth, and plotted in Fig. 2(d) as a function of  $T_{\text{sub}}$ . GaAs(Sb) NWs initially increase the incorporation when temperature is reduced, compared to the growths at 603 °C discussed in Figs. 2(a)–2(c). The number near each point in Fig. 2(d) is the 2D desorption ( $\Gamma_{a_c v}$ ) in percentages of nominal growth rate. The dashed line is the model prediction of incorporation for the GaAs(Sb) samples, based on the adatom conservation model from Eq. (2) (see Supplemental Material S1 [33]) and highlighting a maximum in incorporation around 583 °C for the given growth rate of 0.1 ML/s. None of the samples measured in this series reach nominal incorporation. There are two independent reasons. First, for the two highest temperature samples, the crystal desorption,  $\Gamma_{a_c v}$ , on large mask openings (i.e., 2D-like) is non-negligible and 10% and 5% at 603 °C and 595 °C, respectively (see Supplemental Material S7 for 2D desorption measurements [33]). Second, the source effect term  $\Delta\Gamma_{a_m a_c}$  reduces the incorporation further at lower temperatures as it gets more negative, as seen in the sample grown at 570 °C. This is understood by the decrease of adatom density on the mask due to nucleation of parasitic crystals  $\Gamma_{a_m s}$  near the NWs, leading to an increase of the transition  $\Gamma_{a_c a_m}$ . The parasitic growth on the mask is marked in Fig. 2(d) with the blurred gray background, with a transition happening between 570 °C and 588 °C. Figure 2(e) shows two AFM images

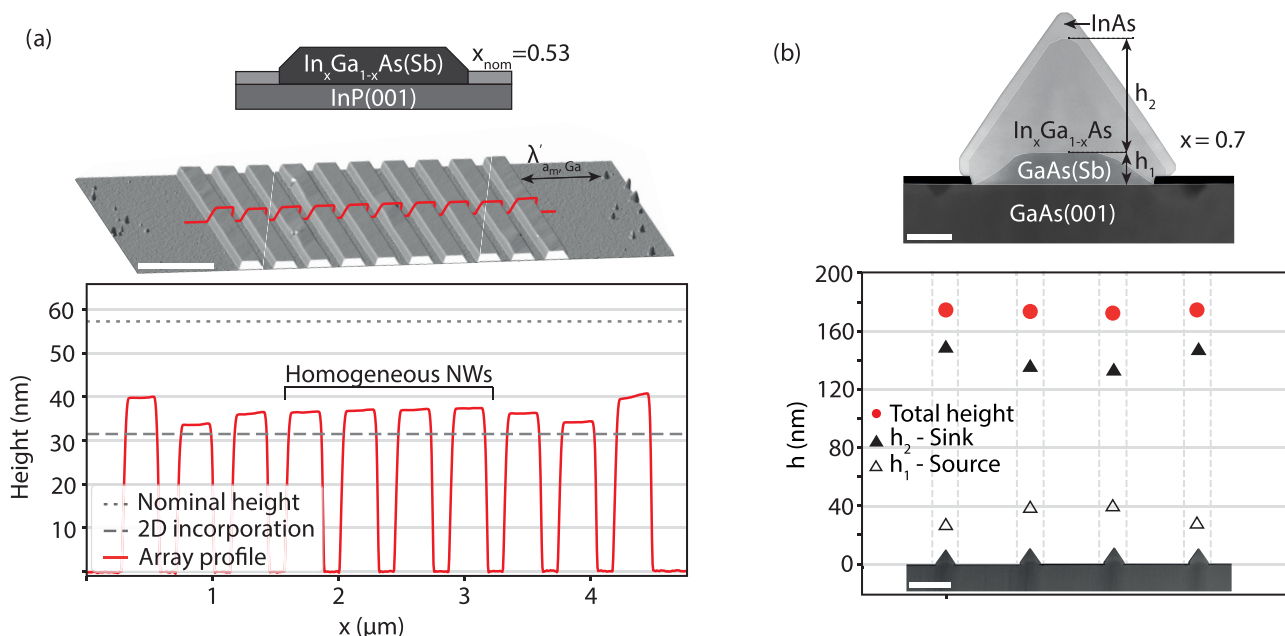


FIG. 4. Engineering arrays of NWs with homogeneous height. (a) Sketch and AFM image of an array of  $\text{In}_{0.53}\text{Ga}_{0.47}\text{As}$  NWs grown on  $\text{InP}(001)$ . In the bottom, AFM line scan across the NWs showing simultaneously both source and sink growth modes, generated by the different group III adatoms. The central NWs of the array form a set of NWs with homogeneous height, due to the formation of an adatom density saturation region. (b) ADF-STEM cross-sectional image of multilayer buffer NWs (top) and low magnification of the NW array (bottom). Material contrast is highlighted for visualization purposes. The plot shows the height of the 2 buffers for each of the 4 NWs in the array, summing up to the same height due to the balanced effect of source and sink growth modes. Scale bars are  $1 \mu\text{m}$  in (a),  $50 \text{ nm}$  in (b) (top), and  $500 \text{ nm}$  in (b) (bottom).

of individual  $\text{GaAs}(\text{Sb})$  NWs from the same growth, with different  $w$ , and separated  $50 \mu\text{m}$  from other mask opening. For the  $45\text{-nm}$ -wide NW, due to the small  $w$ , the term  $\Delta\Gamma_{a_m a_c}/w$  from Eq. (2) is negative enough to override the growth on the substrate due to the dominating  $\Gamma_{a_c a_m}$ , whereas parasitic growth can nucleate on the mask. This would be an extreme case where the design parameter  $w$  induces a negative growth rate for the NW at growth conditions that otherwise induce growth in wider mask openings, as shown in the  $150 \text{ nm}$  wide NW.

The selectivity window for SAG NWs describes suitable growth conditions in the temperature-flux space, as studied by Aseev *et al.* in Ref. [21] for  $\text{GaAs}(001)$  substrates and  $\text{SiO}_2$  mask. Based on our results, we schematically introduce in Fig. 3 the effect on the lower (desorption from the crystal,  $\Gamma_{a_c v}$ ) and upper (nucleation on the mask,  $\Gamma_{a_m s}$ ) boundaries caused by the Sb surfactant, and the NW design limitation on  $w$ . The solid black curves in Fig. 3 represent the upper and lower boundaries and they confine the region in the  $f$ - $T$  space where the growth is selective. From the results presented in Figs. 2(a)–2(d), the effect on these boundaries due to the addition of Sb surfactant is the shift to lower temperatures (or higher fluxes), sketched with solid red lines. It is unclear if the shift is identical for both boundaries since the transition rates defining them might be affected differently by Sb. The growth limitation on the design parameter  $w$  shown in Fig. 2(e) has an implication on the lower boundary by additionally shifting the curve toward lower temperatures by a factor proportional to the strength of the source effect,  $\Delta\Gamma_{a_m a_c}/w$ . This shift can cause the lower boundary to cross the upper boundary,

effectively closing the SAG window as shown in Fig. 2(e). We emphasize that for previously reported SAG  $f$ - $T$  conditions where the  $w$  limitation in source mode was not taken into account, it is possible to override the growth. Next, as demonstrated in Fig. 2(d), the source effect can be reduced by decreasing the growth temperature, until the point where nucleation on the mask starts. Reducing  $f$  while still growing selectively would allow to neutralize the source effect by shifting the incorporation curve in Fig. 2(d) upwards until  $\Gamma_{\text{inc}} = 1$ . In Fig. 3 we speculate the appearance of a sink region at low  $f$  and  $T$  where  $\Delta\Gamma_{a_m a_c} > 0$  and whose boundary gives balance growth mode independent of NW design. The sink window is expected to extend symmetrically beyond the upper boundary toward lower temperatures until the adatom density is sufficiently reduced by nucleation on the mask, entering the source growth mode once more. This localized region in the  $f$ - $T$  selectivity map would imply the existence of a critical flux  $f^*$  above which it would not be possible to achieve a balanced growth. Further exploration is needed at lower group III fluxes and temperatures of the SAG window in order to demonstrate a balanced growth mode and the existence of the sink effect region for binary materials.

## V. ENGINEERING OF III-V TERNARY MATERIALS

Fabrication of SAG NWs for quantum electronic devices usually requires the growth of multistack buffer layers to minimize the generation of defects that degrade electronic properties [12]. Specifically, the growth of  $\text{In}_x\text{Ga}_{1-x}\text{As}$  buffer layers between the substrate and the  $\text{InAs}$  transport channel

has been demonstrated to be beneficial for the strain relaxation of InAs [38]. Using this approach, in Fig. 4 we show two independent methods of engineering arrays of NWs with constant height based on the presented source and sink growth regimes.

Figure 4(a) shows an array of lattice matched  $\text{In}_{0.53}\text{Ga}_{0.47}\text{As}$  NWs grown on InP(001). The three outermost NWs are under the influence of the nearby mask, whereas the four middle NWs have a constant height. This approach to grow several NWs homogeneously can be extended by increasing the number of NWs in the array, generating a central region in each array where adatom density is constant. In Fig. 4(a), the outermost NWs are the highest in the array. This is caused by the different behavior of group III adatoms of the  $\text{In}_{0.53}\text{Ga}_{0.47}\text{As}$  ternary alloy, as opposed to the pure source case from Fig. 2(a). For the growth  $T_{\text{sub}} = 508$  °C and for the given fluxes, we speculate that Ga adatoms are being incorporated in the sink regime of their SAG window, whereas the In adatoms are in source regime simultaneously (see Supplemental Material S2 for growth conditions [33]). This explains a local sink behavior for the outer NWs and a general source effect for the inner NWs compared to the second and third outermost ones.

Another approach of growing reproducible structures is presented in Fig. 4(b). The NWs consist of two buffer layers of GaAs(Sb) and  $\text{In}_{0.7}\text{Ga}_{0.3}\text{As}$  with an InAs transport channel, grown on a GaAs(001) substrate. The annular dark field scanning TEM on Figure 4(b) shows the cross-sectional geometry and contrast between the different layers. Material contrast is highlighted for visualization purposes. The  $\text{In}_{0.7}\text{Ga}_{0.3}\text{As}$  composition is extracted by electron energy loss spectroscopy and its growth temperature dependence and array position variation has been studied in depth in Ref. [38]. The inset in the plot is the cross-sectional lamella of the array in study via focused ion beam milling. The white (black) triangles show the height

of the first (second) buffers. Here a combination of source growth mode from the first buffer and sink growth mode from the second buffer generates an array of NWs with constant height, where the subsequent InAs layer was grown on.

## VI. CONCLUSION

In summary, we have measured and analyzed the SAG growth rates of GaAs, GaAs(Sb), and  $\text{In}_x\text{Ga}_{1-x}\text{As}$  NWs on GaAs/SiO<sub>2</sub> patterned substrates. We show how the growth rates are dominated by the effective flux of adatoms across the mask to crystal areas,  $\Delta\Gamma_{\text{ad}a_c}$ , where the sign of  $\Delta\Gamma_{\text{ad}a_c}$  determines whether the growth is in source (negative), balanced (neutral) or sink (positive) growth mode. The growth mode is determined by measuring the growth rate dependence on the variables: NW array pitch, position, width, crystallographic orientation, and chemical composition. With the growth conditions used in this study, GaAs and GaAs(Sb) grow consistently in source mode while  $\text{In}_x\text{Ga}_{1-x}\text{As}$  grows effectively in sink mode. We demonstrate the possibility of growing reproducible NWs by two different approaches: Tuning the growth mode of each group III species on buffer layer stacks and by increasing the number of NWs in the array, creating uniform incorporation conditions for adjacent NWs.

## ACKNOWLEDGMENTS

The research was supported by Microsoft Quantum Initiative and the European Research Council under the Horizon 2020 research and innovation program, starting grant HEMSDAM, Agreement No. 716655. The authors thank Mohana Rapjalke for valuable discussions and technical support. M.E.C. thanks Elisabetta Fiordaliso for support in microscopy.

- 
- [1] T. D. Stanescu and S. Tewari, *J. Phys.: Condens. Matter* **25**, 233201 (2013).
  - [2] T. Karzig, C. Knapp, R. M. Lutchyn, P. Bonderson, M. B. Hastings, C. Nayak, J. Alicea, K. Flensberg, S. Plugge, Y. Oreg *et al.*, *Phys. Rev. B* **95**, 235305 (2017).
  - [3] S. Plugge, A. Rasmussen, R. Egger, and K. Flensberg, *New J. Phys.* **19**, 012001 (2017).
  - [4] R. M. Lutchyn, J. D. Sau, and S. Das Sarma, *Phys. Rev. Lett.* **105**, 077001 (2010).
  - [5] R. Wagner and W. Ellis, *Appl. Phys. Lett.* **4**, 89 (1964).
  - [6] Y. Kato, S. Kitamura, K. Hiramatsu, and N. Sawaki, *J. Cryst. Growth* **144**, 133 (1994).
  - [7] M. A. Johar, H.-G. Song, A. Waseem, M. A. Hassan, I. V. Bagal, Y.-H. Cho, and S.-W. Ryu, *Appl. Mater. Today* **19**, 100541 (2020).
  - [8] S. Ambrosini, M. Fanetti, V. Grillo, A. Franciosi, and S. Rubini, *J. Appl. Phys.* **109**, 094306 (2011).
  - [9] S. A. Khan, C. Lampadaris, A. Cui, L. Stampfer, Y. Liu, S. J. Pauka, M. E. Cachaza, E. M. Fiordaliso, J.-H. Kang, S. Korneychuk *et al.*, *ACS Nano* **14**, 14605 (2020).
  - [10] M. Hei, E. Riedlberger, D. Spirkoska, M. Bichler, G. Abstreiter, and A. F. i Morral, *J. Cryst. Growth* **310**, 1049 (2008).
  - [11] L. Desplanque, M. Fahed, X. Han, V. Chinni, D. Troadec, M. Chauvat, P. Ruterana, and X. Wallart, *Nanotechnology* **25**, 465302 (2014).
  - [12] F. Krizek, J. E. Sestoft, P. Aseev, S. Marti-Sanchez, S. Vaitiekėnas, L. Casparis, S. A. Khan, Y. Liu, T. Stankevi, A. M. Whitticar *et al.*, *Phys. Rev. Mater.* **2**, 093401 (2018).
  - [13] S. Vaitiekėnas, A. M. Whitticar, M. T. Deng, F. Krizek, J. E. Sestoft, C. J. Palmstrom, S. Marti-Sanchez, J. Arbiol, P. Krogstrup, L. Casparis, and C. M. Marcus, *Phys. Rev. Lett.* **121**, 147701 (2018).
  - [14] G. L. R. Anselmetti, E. A. Martinez, G. C. Menard, D. Puglia, F. K. Malinowski, J. S. Lee, S. Choi, M. Pendharkar, C. J. Palmstrom, C. M. Marcus, L. Casparis, and A. P. Higginbotham, *Phys. Rev. B* **100**, 205412 (2019).
  - [15] L. Desplanque, A. Bucamp, D. Troadec, G. Patriarche, and X. Wallart, *Nanotechnology* **29**, 305705 (2018).
  - [16] M. Fahed, L. Desplanque, D. Troadec, G. Patriarche, and X. Wallart, *Nanotechnology* **27**, 505301 (2016).
  - [17] M. Fahed, L. Desplanque, C. Coinon, D. Troadec, and X. Wallart, *Nanotechnology* **26**, 295301 (2015).
  - [18] G. Tutuncuoglu, M. de La Mata, D. Deiana, H. Potts, F. Matteini, J. Arbiol, and A. F. i Morral, *Nanoscale* **7**, 19453 (2015).

- [19] J. S. Lee, S. Choi, M. Pendharkar, D. J. Pennachio, B. Markman, M. Seas, S. Koelling, M. A. Verheijen, L. Casparis, K. D. Petersson *et al.*, *Phys. Rev. Mater.* **3**, 084606 (2019).
- [20] M. Friedl, K. Cervený, P. Weigele, G. Tütüncüoğlu, S. Martí-Sánchez, C. Huang, T. Patlatiuk, H. Potts, Z. Sun, M. O. Hill *et al.*, *Nano Lett.* **18**, 2666 (2018).
- [21] P. Aseev, A. Fursina, F. Boekhout, F. Krizek, J. E. Sestoft, F. Borsoi, S. Heedt, G. Wang, L. Binci, S. Martí-Sánchez *et al.*, *Nano Lett.* **19**, 218 (2018).
- [22] G. Bacchin and T. Nishinaga, *J. Cryst. Growth* **191**, 599 (1998).
- [23] M. Wimmer, A. Akhmerov, J. Dahlhaus, and C. Beenakker, *New J. Phys.* **13**, 053016 (2011).
- [24] K. Flensberg, *Phys. Rev. B* **82**, 180516(R) (2010).
- [25] Z. Yang, A. Surrente, G. Tutuncuoglu, K. Galkowski, M. Cazaban-Carrazé, F. Amaduzzi, P. Leroux, D. Maude, A. Fontcuberta i Morral, and P. Plochocka, *Nano Lett.* **17**, 2979 (2017).
- [26] M. Fahed, L. Desplanque, D. Troadec, G. Patriarche, and X. Wallart, *J. Cryst. Growth* **477**, 45 (2017).
- [27] P. Aseev, G. Wang, L. Binci, A. Singh, S. Martí-Sánchez, M. Botifoll, L. J. Stek, A. Bordin, J. D. Watson, F. Boekhout *et al.*, *Nano Lett.* **19**, 9102 (2019).
- [28] R. L. O. het Veld, D. Xu, V. Schaller, M. A. Verheijen, S. M. Peters, J. Jung, C. Tong, Q. Wang, M. W. de Moor, B. Hesselmann *et al.*, *Commun. Phys.* **3**, 59 (2020).
- [29] T. Sugaya, Y. Okada, and M. Kawabe, *Jpn. J. Appl. Phys.* **31**, L713 (1992).
- [30] A. Okamoto and K. Ohata, *Appl. Phys. Lett.* **51**, 1512 (1987).
- [31] A. Okamoto and K. Ohata, *J. Appl. Phys.* **66**, 3413 (1989).
- [32] P. Krogstrup, H. I. Jørgensen, E. Johnson, M. H. Madsen, C. B. Sørensen, A. Fontcuberta i Morral, M. Aagesen, J. Nygård, and F. Glas, *J. Phys. D: Appl. Phys.* **46**, 313001 (2013).
- [33] See Supplemental Material at <http://link.aps.org/supplemental/10.1103/PhysRevMaterials.5.094601> for the following details: S1, adatom kinetics models; S2, longitudinal source effect and facet roughness; S3, pregrowth fabrication and characterization; S4, MBE growth recipes; S5, characterization techniques; S6, selectivity between arrays of nanowires; and S7, crystal desorption measurements.
- [34] F. Krizek, Semiconductor nanowire networks grown by molecular beam epitaxy, Ph.D. thesis, Ph.D. School of the Faculty of Science, University of Copenhagen, 2018.
- [35] J. Neave, B. Joyce, P. Dobson, and N. Norton, *Appl. Phys. A* **31**, 1 (1983).
- [36] L. Däweritz and R. Hey, *Surf. Sci.* **236**, 15 (1990).
- [37] A. Guillén-Cervantes, Z. Rivera-Alvarez, M. López-López, E. López-Luna, and I. Hernández-Calderón, *Thin Solid Films* **373**, 159 (2000).
- [38] D. V. Beznasyuk, S. Martí-Sánchez, J.-H. Kang, R. Tanta, M. Rajpalke, T. Stankevič, A. W. Christensen, M. C. Spadaro, R. Bergamaschini, J. Arbiol *et al.*, [arXiv:2103.15971](https://arxiv.org/abs/2103.15971).
- [39] T. Yamamura, T. Matsushita, T. Koitabashi, and T. Kondo, *Jpn. J. Appl. Phys.* **44**, L1397 (2005).
- [40] J. L. Roehl, A. Kolagatla, V. K. K. Ganguri, S. V. Khare, and R. J. Phaneuf, *Phys. Rev. B* **82**, 165335 (2010).
- [41] M. Mińkowski and M. A. Załuska-Kotur, *Phys. Rev. B* **91**, 075411 (2015).
- [42] E. Tournie, N. Grandjean, A. Trampert, J. Massies, and K. Ploog, *J. Cryst. Growth* **150**, 460 (1995).
- [43] C. W. Oh, E. Kim, and Y. H. Lee, *Phys. Rev. Lett.* **76**, 776 (1996).
- [44] A. Okamoto, *Semicond. Sci. Technol.* **8**, 1011 (1993).
- [45] T. Sato, I. Tamai, and H. Hasegawa, *J. Vac. Sci. Technol. B* **22**, 2266 (2004).
- [46] S. Yokoyama, J. Oogi, D. Yui, and M. Kawabe, *J. Cryst. Growth* **95**, 32 (1989).